ACS OMEGA

http://pubs.acs.org/journal/acsodf

Article

Partial Pressure Assisted Growth of Single-Layer Graphene Grown by Low-Pressure Chemical Vapor Deposition: Implications for High-Performance Graphene FET Devices

Indu Sharma,* Girija Shankar Papanai, Sharon Jyotika Paul, and Bipin Kumar Gupta*

Cite This: *ACS Omega* 2020, 5, 22109−22118

Read Online

ACCESS | Metrics & More | Article Recommendations | Supporting Information

ABSTRACT: An attempt has been made to understand the thermodynamic mechanism study of the low-pressure chemical vapor deposition (LPCVD) process during single-layer graphene (SLG) growth as it is the most debatable part of the CVD process. The intensive studies are being carried out worldwide to enhance the quality of LPCVD-grown graphene up to the level of mechanically exfoliated SLG. The mechanism and processes have been discussed earlier by several research groups during the variation in different parameters. However, the optimization and mechanism involvement due to individual partial pressure-based effects has not been elaborately discussed so far. Hence, we have addressed this issue in detail including thermodynamics of the growth process and tried to establish the effect of the partial pressures of individual gases during the growth of SLG. Also, optical microscopy, Raman spectroscopy, and atomic force microscopy (AFM) have been performed to determine the quality of SLG. Furthermore, nucleation density has also been estimated to understand a plausible mechanism of graphene growth based on partial pressure. Moreover, the field-effect transistor (FET) device has been fabricated to determine the electrical properties of SLG, and the estimated mobility has been found as ~2595 $cm^2 V^{-1} s^{-1}$ at $n = -2 \times 10^{12}$ cm^{-2}. Hence, the obtained results trigger that the partial pressure is an important parameter for the growth of SLG and having various potential applications in high-performance graphene FET (GFET) devices.

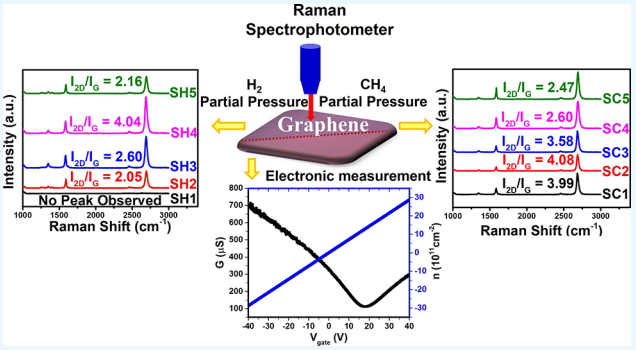

1. INTRODUCTION

Graphene, the first two-dimensional (2D) material having sp^2 hybrid carbon atoms placed in the honeycomb lattice structure, brings boom in the electronic industry due to its astonishing electronic, physical, chemical and mechanical properties. The linear band structure of graphene makes it a plausible material for approaching the stepping stone goal toward graphene-based devices in the market for commercialization. Graphene has electronic mobility 100 times more than that of silicon.[1−4]

Thus, graphene can be used for high-tech applications in the field of electronics.[5] Although several methods such as mechanical exfoliation,[6,7] chemical exfoliation (Hummer's method),[8−10] sublimation of SiC,[2,11,12] and chemical vapor deposition (CVD)[13−19] have been introduced in the research as well as industrial field to synthesize small area (μm^2) to large area (cm^2) graphene, CVD is the unsurpassed method to produce scalable high-quality graphene. The quality of graphene depends upon continuity of the graphene layer with less grain boundaries. Hence, less scattering of charge carriers occurs at defects and grain boundaries. In that respect, however, the quality of mechanically exfoliated graphene is high, but yield/scalability is very less, which limits the use of mechanically exfoliated graphene for industrial applications. Hence, mechanically exfoliated graphene is only limited to the for study of the fundamental investigation of different properties of graphene. On the other hand, impurity issue is unified during graphene growth by Hummer's method. However, yield is more in this case; therefore, Hummer's method is more suitable to use for composite applications. Among all of the synthesis methods, CVD is the most suitable method for producing scalable high-quality graphene for graphene field-effect transistor (GFET) applications.

Due to the self-limiting behavior of copper (Cu) and the less solubility of carbon in a copper substrate (<0.001 atom %), graphene growth is limited only to the surface of the copper substrate, which insists growth of uniform single-layer graphene (SLG). Hence, several research groups used copper as a catalyst to get SLG during the growth of graphene.[13−15] Other metals also lead to formation of graphene, but multiple-

Received: May 8, 2020
Accepted: August 13, 2020
Published: August 26, 2020

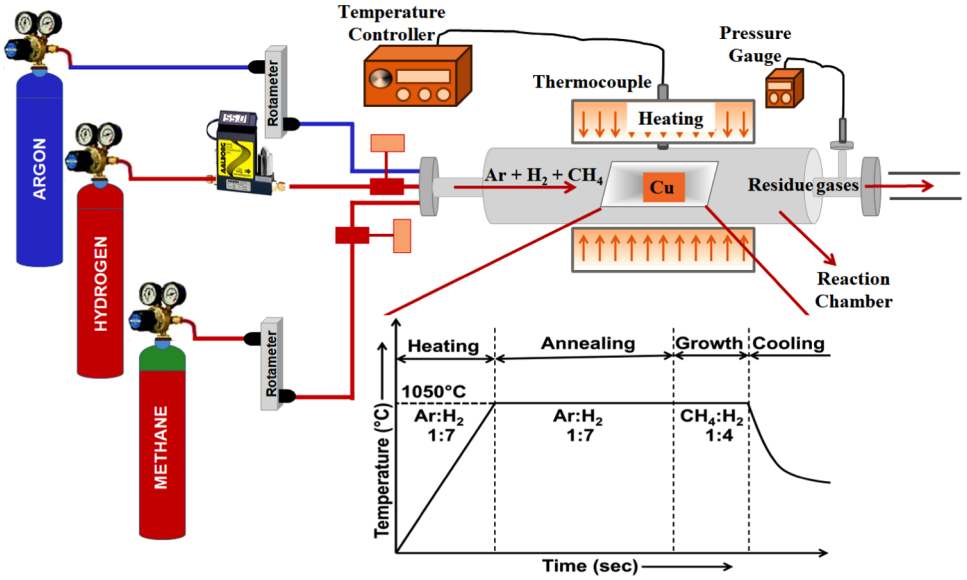

Figure 1. Schematic of the LPCVD setup showing the temperature profile of graphene growth.

layer formation or uniformity is the major issue with other catalysts.[13−20] CVD graphene is polycrystalline in nature because of coalescence of graphene nuclei formation and growth of these nuclei during synthesis by CVD. Coalescence of graphene grains results in formation of grain boundaries that act as scattering sites for charge carriers and degrade the quality of graphene. Quality enhancement can be achieved by decreasing nucleation density during graphene growth by the CVD method. Several efforts have been made till now to control the nucleation density of graphene grain.[21−26]

Like numerous parameters (annealing temperature, growth temperature, growth time, gas flow rates, etc.) during graphene growth by CVD, pressure is a portentous parameter that controls the growth and quality of graphene. Several research groups studied both atmospheric pressure chemical vapor deposition (APCVD) and low-pressure chemical vapor deposition (LPCVD) methods to synthesize graphene. Chances of getting single-layer graphene (SLG) in LPCVD is high,[27] whereas in the case of APCVD, multiple layers of graphene are formed on the catalytic surface during growth. A proper understanding of multiple steps involved in the growth of graphene is the essential part of high-quality graphene formation. Pressure is related to quality in terms of graphene grains, which could be affected by the change in nucleation density. Hence, in this report, we focused mainly on synthesis of graphene on a copper catalytic surface where diffusion of gases was involved, and the effect of the partial pressures of both source gas (CH_4) and co-catalytic gas (H_2) on graphene quality was studied.

2. RESULTS AND DISCUSSION

Graphene has been synthesized by using indigenously developed LPCVD set up as shown in Figure 1 and Table 1 shows samples with different individual gas partial pressure of methane as well as hydrogen during graphene growth (for more details see materials and methods section). Various analytic tools were used to investigate the quality, surface morphology, and electronic features of SLG grown at different partial pressures. Estimation of the presence of SLG has been performed by contrast (C) from the captured optical

Table 1. Different Samples with Different Partial Pressure of Gases during CVD Graphene Growth

	variation of hydrogen partial pressure			variation of methane partial pressure	
sample	hydrogen pressure P_{H_2} (Torr)	methane pressure P_{CH_4} (Torr)	sample	hydrogen pressure P_{H_2} (Torr)	methane pressure P_{CH_4} (Torr)
SH1	0.5 ± 0.2	12 ± 0.2	**SC1**	13 ± 0.2	7 ± 0.2
SH2	3 ± 0.2	12 ± 0.2	**SC2**	13 ± 0.2	12 ± 0.2
SH3	8 ± 0.2	12 ± 0.2	**SC3**	13 ± 0.2	22 ± 0.2
SH4	13 ± 0.2	12 ± 0.2	**SC4**	13 ± 0.2	32 ± 0.2
SH5	18 ± 0.2	12 ± 0.2	**SC5**	13 ± 0.2	42 ± 0.2

micrographs of graphene on the Si/SiO_2 substrate using the contrast equation: $C = (I_{substrate} - I_{graphene})/I_{substrate}$, where $I_{substrate}$ is the reflected light intensity by the substrate and $I_{graphene}$ is the reflected light intensity by graphene. Here SiO_2 of thickness 300 nm has been used on silicon as it gives the maximum optical contrast in the visible range of the electromagnetic spectrum due to constructive interference. Visibility of graphene on the Si/SiO_2 substrate also depends upon the experience of the observer. Color contrast in our case lies in blue color on the Si/SiO_2 (300 nm) substrate having 300 nm SiO_2 thickness and it can be changed from one lab to other lab.[28,29]

Figure 2 depicts the optical images of SLG produced by the indigenously developed LPCVD setup. Representative optical images of graphene on a copper foil and Si/SiO_2 substrate are shown in Figure 2a−d. Optical micrographs of the as-received catalytic copper foil noticeably demonstrate the presence of processing lines generated during the rolling process (Figure 2a), annealing results in enlargement of copper grains as a result of recrystallization of the copper foil (Figure 2b,c), and the difference in color contrast of graphene from that of Si/SiO_2 (Figure 2d,e) shows successful transfer of clean and wrinkle-free graphene from the catalytic copper surface to the Si/SiO_2 substrate. Uniform graphene contrast can be clearly seen at low and high magnification, as shown in Figure 2d−f, which depicts the growth of the large area of continuous graphene. Edges and torn graphene are labeled in Figure 2d−f

https://dx.doi.org/10.1021/acsomega.0c02132
ACS Omega 2020, 5, 22109−22118

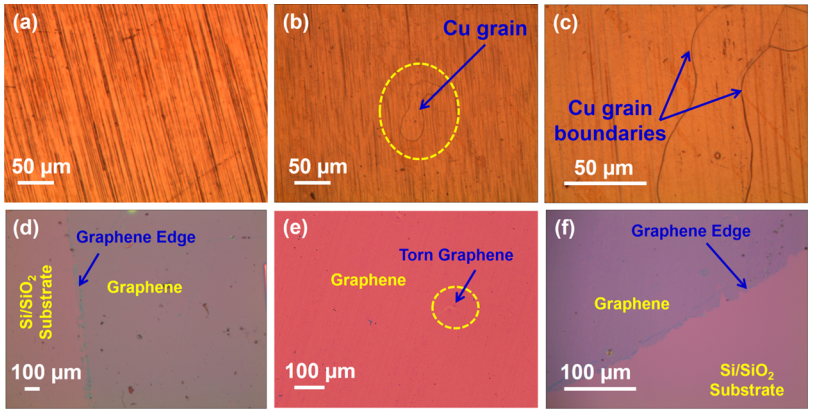

Figure 2. Optical images of (a) as-received copper foil (resolution 20×), (b, c) graphene covered copper foil showing grain boundaries at different resolutions (20× and 50×, respectively), and (d–f) graphene on the Si/SiO_2 substrate after the transfer process at different resolutions (5×, 10× and 20×, respectively) (sample SC2).

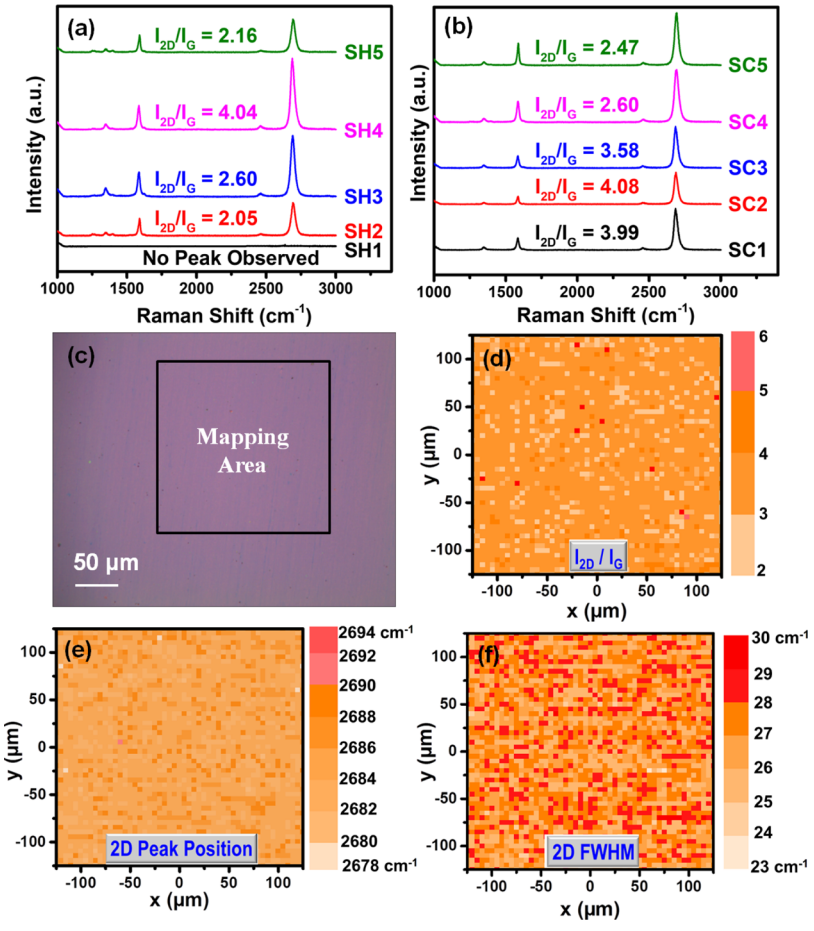

Figure 3. (a, b) Raman spectra of CVD graphene after transfer on the Si/SiO_2 substrate at different (a) hydrogen partial pressures (SH1–SH5) and (b) methane partial pressures (SC1–SC5). (c–f) Raman mapping of the marked area (250 μm × 250 μm) in (c) optical image of graphene, (d) intensity ratio map, (e) 2D peak position map, and (f) 2D full width half maxima of graphene (sample SC2).

to show different color contrasts of graphene on the Si/SiO_2 substrate.

Figure S1 shows optical micrographs of different samples after transfer on the Si/SiO_2 substrate. Figure S1a–e depicts the optical images of graphene on increasing the hydrogen gas partial pressure, whereas Figure S1f–j depicts the optical images of graphene on changing the methane gas partial pressure. No graphene is observed at the lowest hydrogen partial pressure (sample SH1); as we increase the partial pressure of hydrogen, there is a continuous growth of graphene till sample SH4, and as we further increase the partial pressure of hydrogen, etching of graphene from few areas starts, which results in discontinuity of the graphene sheet from areas marked by yellow arrows. On the other hand, continuous graphene growth has been observed in all of the samples irrespective of whether the partial pressure of graphene was low or high.

https://dx.doi.org/10.1021/acsomega.0c02132
ACS Omega 2020, 5, 22109–22118

Table 2. Comparative Raman Data Analysis of Graphene at Different Hydrogen Partial Pressures (SH1−SH5) and Methane Partial Pressures (SC1−SC5)

$P(H_2)$ (Torr)					$P(CH_4)$ (Torr)				
sample	position	I_{2D}/I_G	2D (FWHM)	I_D/I_G	sample	position	I_{2D}/I_G	2D (FWHM)	I_D/I_G
SH1					SC1	G ∼ 1585, 2D ∼ 2681	∼3.99	∼31	∼0.1
SH2	G ∼ 1587, 2D ∼ 2691	∼2.05	∼37	∼0.1	SC2	G ∼ 1585, 2D ∼ 2680	∼4.08	∼29	∼0.1
SH3	G ∼ 1588, 2D ∼ 2687	∼2.60	∼35	∼0.4	SC3	G ∼ 1585, 2D ∼ 2681	∼3.58	∼31	∼0.1
SH4	G ∼ 1586, 2D ∼ 2681	∼4.04	∼30	∼0.1	SC4	G ∼ 1585, 2D ∼ 2681	∼2.60	∼34	∼0.1
SH5	G ∼ 1587, 2D ∼ 2690	∼2.16	∼36	∼0.1	SC5	G ∼ 1585, 2D ∼ 2687	∼2.47	∼36	∼0.1

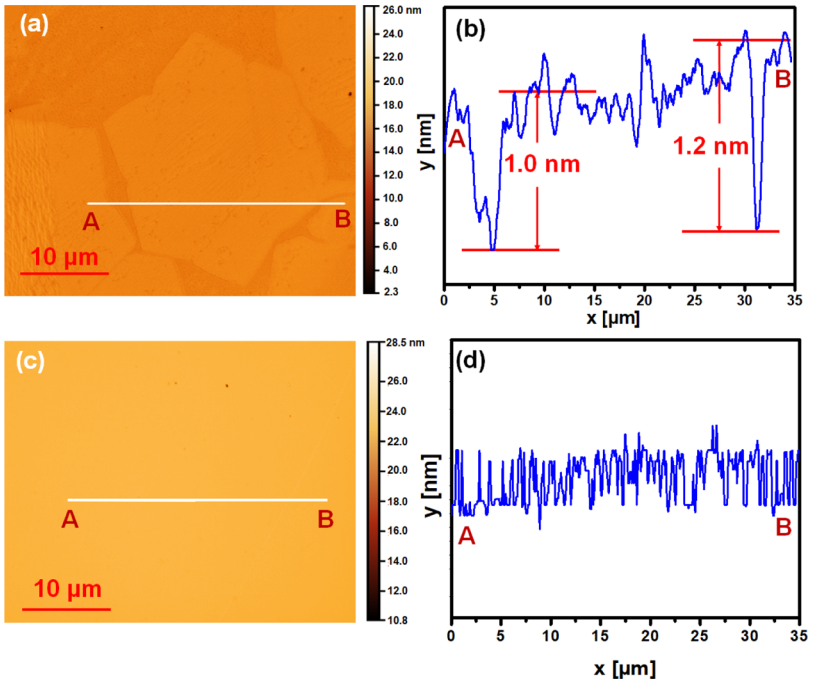

Figure 4. (a, b) AFM image with the height profile of (a, b) graphene grain and (c, d) continuous graphene on the Si/SiO_2 substrate (sample SC2).

Raman spectroscopy is a primary flexible technique to ensure the graphene quality. For further quality observations, all of the samples were analyzed by Raman spectroscopy. First-order Raman scattering occurs at the Brillouin zone (BZ) center and due to the E_{2g} doubly degenerate phonon mode, gives the G band at 1580 cm^{-1} and signifies the presence of sp^2 symmetry in the graphene sheet.[30] Further, interruption in breathing of six atomic rings of hexagon present in graphene gives the D band at 1350 cm^{-1}, which is generated as a result of the transition from transverse optical (TO) phonons around the BZ corner K. Furthermore, the 2D band at 2700 cm^{-1} is the overtone of the D band, and it is totally independent of crystal disorderness. D band intensity signifies the presence of defects in the graphene crystal structure, whereas 2D band intensity or broadness is truly related to the number of layers present in graphene.[30,31] Moreover, the I_D/I_G and I_{2D}/I_G ratios give the measure of the presence of the amount of defects and number of layers respectively. The I_{2D}/I_G ratio > 2 signifies the presence of single-layer graphene, the I_{2D}/I_G ratio = 1 signifies the presence of bilayer graphene, and the I_{2D}/I_G ratio <1 signifies the presence of trilayer/few-layer/multilayer graphene. The full width half maxima (FWHM) of both the peaks of G and 2D ensure the results as the FWHM for single-layer graphene is <35 cm^{-1} where only one transition is possible and the FWHM for bilayer or multilayer graphene is >35 cm^{-1} where four transitions are possible. Figure 3a,b demonstrates the Raman spectra of graphene with varying partial pressures of H_2 and CH_4. It is found by the I_{2D}/I_G ratio that the quality of graphene grown is high for samples SC2 and SH4 (at 13 ± 2 and 12 ± 2 Torr partial pressures of H_2 and CH_4, respectively). Moreover, at low hydrogen partial pressure and at high methane partial pressure, the quality of graphene degrades. Raman spectroscopic results and graphene uniformity were confirmed by Raman mapping of graphene sample SC2 where the Raman map was performed on 250 μm × 250 μm area with a step size of 5 μm, as shown in the black square area in Figure 3c. Figure 3d−f shows the signature of uniformity of SLG on the Si/SiO_2 substrate as the I_{2D}/I_G ratio >3, $2D_{peak\ position}$ 2680−2684 cm^{-1}, and $2D_{FWHM}$ ∼27−29 cm^{-1}.

Optical micrographs and Raman spectrum manifested that at very low hydrogen partial pressure there is no growth of graphene on the substrate. In other cases, like for different hydrogen and methane partial pressures, there is growth of graphene; however, the quality varies as shown by the I_{2D}/I_G ratio in Raman spectra (Figure 3). Calculated peak positions, I_{2D}/I_G, I_D/I_G, and $2D_{FWHM}$ values for each Raman spectrum are given in Table 2, where the I_D/I_G ratio in all cases is <0.5, which signifies negligible defects in graphene grown by LPCVD.

After optical and Raman examination, samples SC2 have been explored using atomic force microscopy (AFM). The thickness and uniformity of the graphene film are confirmed by

https://dx.doi.org/10.1021/acsomega.0c02132
ACS Omega 2020, 5, 22109−22118

AFM, as shown in Figure 4a,b and 4c, d, respectively. Figure 4a shows graphene grains, and Figure 4b shows the height profile of graphene, which shows two dips at the edges of graphene grain and the height of these dips shows the thickness of graphene. Theoretically, the thickness of graphene is 0.345 nm, but here results show the thickness of ∼1 nm. The theoretically and experimentally extracted thickness difference is due to adsorption of air or water molecules on graphene during the transfer process and change in cohesive forces between the substrate and graphene films. AFM instrument offset also has an added impact toward showing more than the expected thickness of the graphene film. Figure 4c and 4d shows uniformity of graphene as there is no dip shown in the height profile of continuously grown graphene.

In the LPCVD process, nucleation and growth are the main steps that control the graphene size and quality. In this LPCVD process, graphene is synthesized by decomposition of methane on a catalyst in the presence of H_2 at high temperature. Here, methane is used as a source rather than ethane, propane, acetylene, and ethylene as it has the lowest C atom among all of the hydrocarbons and has higher decomposition temperature.[32] This elicits the methane biddable gas source for deposition of single-layer graphene rather than multilayer formation. the understanding of both thermodynamics and kinetics of the CVD process is equally important for graphene growth. In our study, both kinetics and thermodynamics of graphene growth have been studied to enhance the graphene quality by LPCVD. During the LPCVD process, nucleation occurs when carbon atoms diffuse on the catalytic surface having low surface energy. Diffusion of gases depends upon the number of collisions occurring during the reaction.[27] Surface energy helps in dominating the nucleation process of graphene during growth. In other words, nucleation rate is determined by surface energy. Low surface energy leads to formation of a fewer number of nuclei. It further leads to the growth of graphene with less grain boundaries that act as scattering sites for charge carriers and hence promote the growth of high-quality graphene. Further, diffusion totally depends upon collision of gases on the surface of the copper substrate. Methane decomposes on the catalytic surface at high temperature to form carbon radicals, and these carbon radicals diffuse onto the copper surface to form graphene lattice. Diffusion coefficient at given temperature T and pressure P depends on the number of moles of gas molecules or on molecular weights of gas species.[33] Other than the number of moles, diffusion collision integral is another factor on which diffusion coefficient depends. Diffusion coefficient for each sample has been calculated using the equation[33]

$$D_{C,H} = \frac{0.0026T^{3/2}}{PM_{C,H}^{1/2}\sigma_{C,H}^{2}\Omega_D} \quad (1)$$

where $M_{C,H} = 2[(1/M_C) + (1/M_H)]^{-1}$. M_C and M_H are molecular weights of gas species methane and hydrogen, respectively. $\sigma_{C,H} = (\sigma_C + \sigma_H)/2$, with σ_C and σ_H being characteristic Lennard-Jones lengths of methane and hydrogen species, respectively. Ω_D is the dimensionless diffusion collision integral. The calculated diffusion coefficient values of gas species are given in Table 3.

Further, nucleation is followed by growth where carbon atoms get accumulated on the edges of graphene and cover the copper surface to give continuous graphene as it takes less time to coalesce two graphene domains. Both steps, nucleation and growth, affect the continuity of graphene and formation of grain boundaries. Hence, nucleation activation energy becomes pretentious by the copper orientation as well as by the H_2/CH_4 ratio but perceptibly affected by change in pressure. Many processes occur on the copper surface during graphene growth that is accountable for different nucleation density[34] including the following steps:[27]

(i) precursor gases diffuse via the boundary layer in the range of the catalytic surface,
(ii) adsorption of precursor gases on the copper substrate,
(iii) dehydrogenation or decomposition reaction results in creation of active carbon species,
(iv) diffusion of resulting carbon atoms on the copper surface to custom graphene lattice,
(v) formation of critical size nuclei, and
(vi) originated critical sized nuclei strive with desorption followed by diffusing away residue gases.

Table 3. Calculated Diffusion Coefficient $D_{C,H}$ for Different Hydrogen Partial Pressures (SH1−SH5) and Methane Partial Pressures (SC1−SC5)

$P(H_2)$ (Torr)		$P(CH_4)$ (Torr)	
sample	diffusion coefficient $D_{C,H}$	sample	diffusion coefficient $D_{C,H}$
SH1	10.19	SC1	0.72
SH2	1.69	SC2	0.42
SH3	0.63	SC3	0.23
SH4	0.39	SC4	0.15
SH5	0.28	SC5	0.12

The quality of SLG depends upon grain boundaries present in graphene, which act as scattering sites for charge carriers. Grain boundaries play a crucial role in scattering of charge carriers. Hence, controlling grain density leads to high-quality graphene,[35,36] which can be analyzed by Raman spectroscopy. Nucleation and growth are major steps during decomposition of methane in CVD growth of graphene. The continuous uniform layer of graphene with the less number of nuclei is more favorable for high-quality graphene growth. Further, nucleation of 2D graphene grains depends on Gibb's free energy ΔG, which is given by[37]

$$\Delta G = E_0 + \sqrt{(6N)} \times E_{Edge} - N \times \Delta\mu_C \quad (2)$$

where E_0 is constant that represents the difference in energy between sp^2 hybridized carbon in a perfect graphene lattice and in the carbon cluster, E_{Edge} is the energy of formation for each edge carbon atom, N is the number of carbon atoms in the cluster, and $\Delta\mu$ is the chemical potential difference of atoms in the carbon cluster and atoms in the graphene lattice.

Hence, nucleation of the graphene domain having the nucleation size r^* and energy barrier for graphene nucleation ΔG^* is

$$\Delta G^* = E_0 + \frac{6E_{edge}^2}{4\Delta\mu_C} \quad (3)$$

and

$$r^* = \frac{3E_{edge}^2}{2\Delta\mu_C} \quad (4)$$

and nucleation rate I is given by

https://dx.doi.org/10.1021/acsomega.0c02132
ACS Omega 2020, 5, 22109−22118

Table 4. Calculated Values of μ_H, μ_{CH_4}, χ, and $\Delta\mu_C$ for Graphene Samples

$P(H_2)$ (Torr)				$P(CH_4)$ (Torr)			
sample	μ_{H_2}	χ	$\Delta\mu_C$	sample	μ_{CH_4}	χ	$\Delta\mu_C$
SH1	1.01	3.18	−11.82	SC1	−11.89	−0.62	13.56
SH2	−0.91	1.39	−8.17	SC2	−11.83	−0.08	13.50
SH3	−0.85	0.40	−8.39	SC3	−11.76	0.53	13.43
SH4	−0.83	−0.08	−8.50	SC4	−11.72	0.90	13.39
SH5	−0.81	−0.40	−8.57	SC5	−11.69	1.17	13.36

$$I \propto I_0 \exp\left(-\frac{\Delta G^*}{kT}\right) \quad (5)$$

where I_0, k, and T are nucleation constant, Boltzmamm constant, and growth temperature, respectively.

Chemical potential is the main factor, as indicated in eqs 2−4, that affects Gibb's free energy and hence nucleation during graphene growth. Again, chemical potential ($\Delta\mu$) depends on pressure (P) and temperature (T) as given by the expression $\Delta\mu = \mu_0 + kT \ln(P/P_0)$.[37] In the LPCVD process, temperature and pressure are two main parameters that affect the chemical potential and hence the nucleation rate of graphene formation.

Several reports focused on the temperature effect on graphene growth, and there are very few reports where a pressure-based study has been reported. The temperature effect on graphene growth has been reported previously.[38] Therefore, in the present work, our main emphasis is on the pressure-based graphene growth study. Here, methane gas pressure and hydrogen gas pressure been varied to observe the effect of partial pressures of both gases on the growth and quality of graphene, and it has been found that the quality increases slightly by increasing hydrogen pressure whereas it decreases by increasing methane pressure, as shown in Figure 4. This can be explained on the basis of the chemical potential of hydrogen as well as the chemical potential of methane. An expression for the chemical potential of hydrogen is given by[39]

$$\mu_H = -0.975 + 0.056 \ln \frac{P_{H_2}}{P_0} \quad (6)$$

and that of the chemical potential of methane is

$$\mu_{CH_4} = -12.102 + 0.112 \ln \frac{P_{CH_4}}{P_0} \quad (7)$$

where P_0, P_{H_2}, and P_{CH_4} are the reference pressure, partial pressure of hydrogen, and partial pressure of methane, respectively. If χ is the P_{CH_4}/P_{H_2} ratio, then under equilibrium conditions, the chemical potential of C and H is given by the relationship[39]

$$\Delta\mu_C = -2\mu_H - 10.152 + 0.112 \ln \chi \quad (8)$$

We have calculated the values of μ_H, μ_{CH_4}, and $\Delta\mu_C$ for all of the samples, which are tabulated in Table 4.

As indicated in Table 4, the partial pressure ratio χ for samples varies with the change in the partial pressure of hydrogen as well as the change in the partial pressure of methane. It can be observed that as we increase the partial pressure of hydrogen, the χ ratio decreases. Hence, the nucleation size increases as calculated from eqs 4 and 8. On the other hand, the χ ratio increases as we increase the partial pressure of methane. Hence, the nucleation size decreases as calculated from eqs 4 and 8. Elliptically, nucleation density decreases as the hydrogen partial pressure increases and nucleation density increases as the methane partial pressure increases.

Experimentally, SLG grain nucleation density has been calculated by reducing growth time to 2 min. The scanning electron microscopy (SEM) of all samples has been performed on CVD-grown graphene grains for the growth time 2 min (optimized time duration). Figure S2 shows the SEM micrographs of graphene grains of different sizes in various samples after graphene nucleation. Nucleation density has been calculated from these SEM micrographs (Figure S2) and is tabulated in Table ST1. Further, Figure S2 shows the growth of different grains with different grain shapes and sizes up to the maximum grain size of ∼100 μm. The grain size increases after increasing the hydrogen partial pressure from SH2 to SH3 and then to SH4. With a further increase in the hydrogen partial pressure to SH5, the grain size starts decreasing (Figure S2a−e). This may be due to the etching effect of hydrogen gas during growth. In another set of samples, with increasing methane gas partial pressure, the size increases from SC1 to SC2 and then to SC3 (Figure S2f−h). Afterwards, with a further increase in the methane gas partial pressure, the number of grains increases and the grain size decreases, and a very small grain size of around 3−4 μm has been observed, as shown in Figure S2j. Decomposition of methane gas at high temperature leads to formation of active species CH*, CH_2*, and CH_3* either as carbanion or radicals. All of these active species lead to formation of graphene nuclei up to certain methane partial pressure depending upon undersaturation, saturation, and oversaturation of the copper substrate. In the undersaturation condition of copper, no nucleation occurs even in the presence of methane. Further, nucleation starts when the copper surface gets saturated. After that, these nuclei grow further when the copper surface gets oversaturated. All of the CH*, CH_2*, and CH_3* radicals are responsible for the growth of graphene in the present case (Figure S2f−h). But after a certain limit of the methane partial pressure, these conditions are not responsible for the growth of graphene as under high pressure of methane gas these CH_2* and CH_3* radicals come out as residue gases without reacting with the copper substrate, which leads to a decrease in the grain size of graphene. Only the CH* radical is responsible for graphene growth in that case. Hence, there is a decrease in graphene grain size, as shown in Figure S2i,j. In other words, we can say that number of moles of gas molecules is responsible for the growth of graphene grains on the copper substrate. In our experiments, growth temperature remains constant and the pressure of gases varies. The number of moles of gas molecules can be varied by changing gas pressure as the number of moles of gas molecules is directly proportional to gas pressure and calculated as shown in Table 5.[40]

https://dx.doi.org/10.1021/acsomega.0c02132
ACS Omega 2020, 5, 22109−22118

Table 5. Calculated Number of Moles n for Different Hydrogen Partial Pressures (SH1−SH5) and Methane Partial Pressures (SC1−SC5)

$P(H_2)$ (Torr)		$P(CH_4)$ (Torr)	
sample	number of moles of gases species, n ($\times 10^{-5}$)	sample	number of moles of gases species, n ($\times 10^{-5}$)
SH1	2.06	SC1	28.85
SH2	12.36	SC2	49.47
SH3	32.98	SC3	90.70
SH4	53.59	SC4	131.93
SH5	74.21	SC5	173.16

When we increase the methane gas partial pressure, more methane molecules diffuse on the surface of copper and growth of graphene grains increases (Figure S2f−h). But this growth is limited up to certain level due to the available surface area of the copper catalyst. As we further increase the methane gas partial pressure, diffusion becomes so fast that more secondary nuclei start to form and leads to an increase in nucleation density. Hence, no more surface of copper remains free for further growth of nuclei, which leads to a small size of graphene grains (Figure S2i,j). High-quality graphene requires less grain boundaries originated due to the large grain size of graphene that has been obtained in sample SH4 or SC2. Further these graphene nuclei have been characterized using Raman spectroscopy and Raman spectra, as shown in Figure S3. It is found that the trend of quality of graphene grains is the same as shown by Raman spectroscopic results of continuously grown graphene, as shown in Figure 3a,b, and the I_{2D}/I_G ratio is above 2 in all samples, which reveals about the growth of single-layer graphene. The single layer of graphene grains is attributed from peak positions, I_{2D}/I_G, I_D/I_G, and $2D_{FWHM}$ values for each Raman spectrum, as calculated in Table S2.

Figure 5 shows the variation of nucleation density with the partial pressure of gases where minimum nucleation density

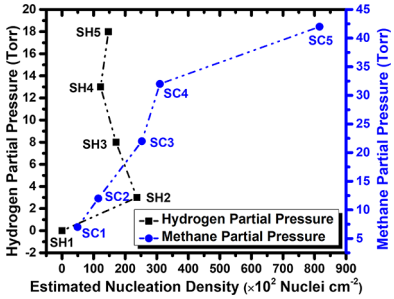

Figure 5. Nucleation density of graphene with variation in hydrogen partial pressure (SH1−SH5) and methane partial pressure (SC1−SC5) (sample SC2).

has been observed for SC1 and SH4. For sample SH1, no graphene nuclei formation occurs due to the high χ ratio, as indicated in Table 4. Again, for sample SH5, nucleation density slightly increases due to the dual nature of hydrogen. In this case, hydrogen acts as both co-catalyst and etchant.[41,42] The methane partial pressure enhances the nucleation density by increasing partial pressure, and experimental results are in accordance with the calculated values of nucleation density according to Table 4 and eq 4. In totality, this process is in favor of high-quality graphene growth at low methane partial pressure due to a lower deposition rate, decreasing nucleation density centers followed by grain growth and suppression of formation of multilayer graphene. Hence, it leads to growth of high-quality graphene after complete coverage on the surface of the copper catalyst after 15 min of growth time, which is confirmed by Raman spectroscopy in Figure 3. Figure 5 shows nucleation density variation with respect to the partial pressure of hydrogen and the partial pressure of methane. It can be observed that there is a slight change in nucleation density as the hydrogen partial pressure increases from SH2 to SH5, and a large change in nucleation density can be observed by increasing the partial pressure of methane from SC1 to SC5. Hence, the most important step during growth is to carefully control the methane partial pressure for getting fewer nuclei on the substrate to get high-quality SLG.

For the measurements of electrical properties, the FET device has been fabricated using electron beam lithography and oxygen plasma etching techniques with dimensions 6 μm x 2 μm. The SEM image of the device is shown in the inset of Figure 6.

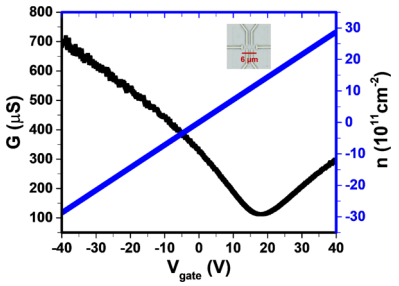

Figure 6. Conductance and number of charge carriers with application of gate voltage on the graphene device (sample SC2).

Resistance measurement is performed at room temperature using the lock-in technique, and a gate voltage of ±40 V is applied. The sheet resistance varies with application of gate voltage, as displayed in Figure 6. The shift in Dirac point at ∼18 V indicates hole doping of graphene, which may be incorporated during transfer using the wet chemical etching process. This indicates that not only grain boundaries affect the scattering of charge carriers[43] but also transfer or any chemical process involved is responsible for degradation of the quality of graphene.[43,44] The carrier mobility calculated by the Drude model $\mu = 1/(ne\rho)$, where n denotes carrier density, e denotes charge carrier, and ρ denotes resistivity.[45] The calculated carrier density n is plotted with application of gate voltage, as shown in Figure 6, and hence the calculated carrier mobility is found to be ∼2595 cm^2 V^{-1} s^{-1} at $n = -2 \times 10^{12}$ cm^{-2}.

3. CONCLUSIONS

High-quality single-layer graphene has been successfully synthesized by the LPCVD method. First, the effect of individual partial pressure during the growth of graphene has been discussed and optimized to get high-quality single-layer graphene. A detailed thermodynamic study of graphene growth while controlling partial pressure of precursor and co-catalytic gases has been carried out. Furthermore, optical microscopy, Raman spectroscopy, and atomic force microscopy (AFM) have been demonstrated to confirm the quality of single-layer graphene. The high quality of single-layer graphene with the I_{2D}/I_G ratio ∼4 with FWHM at ∼29 cm^{-1} has been confirmed by Raman spectroscopy. Furthermore, results are evidenced and demonstrated using the diffusion mechanism. The quality

https://dx.doi.org/10.1021/acsomega.0c02132
ACS Omega 2020, 5, 22109−22118

of single-layer graphene under different partial pressure conditions exhibits the nucleation density ranging from ∼816 × 10^2 to 49 × 10^2 nuclei cm^{-2}. The estimated mobility of single-layer graphene has been found as ∼2595 cm^2 V^{-1} s^{-1} at $n = -2 \times 10^{12}$ cm^{-2}. Thus, the above results suggest that the optimization of partial pressure leads to high-quality electronic grade reproducible graphene that has a real impact on the design of the high-performance GFET devices.

4. EXPERIMENTAL METHODS

4.1. Synthesis of Graphene. A 25 μm thick copper foil with size 4 cm × 4 cm was positioned in the center of a quartz reactor (diam −60 mm) placed on a quartz plate in the isothermal zone of the indigenously developed LPCVD setup (Figure 1). Further, the quartz tube was evacuated to 1 Torr to maintain low pressure inside the quartz reactor, and finally, the mixture of hydrogen and argon gases was incorporated through one side of the tube. Here, the flow of hydrogen gas was maintained at a flow rate of 50 ± 1 sccm through the use of a mass flow meter, and flow of argon gas was maintained by a rotameter, as mentioned in our previously reported paper.[20] After controlling the desirable pressure inside the tube, heating was performed at a rate of 3° min^{-1} up to the temperature of 1050 °C. Hydrogen gas helps to reduce the thin oxide layer present on the copper surface, and argon acts as a carrier gas to activate the catalytic copper substrate. Annealing of catalytic copper was performed for 30 min in the presence of both hydrogen and argon gases. Subsequently, methane gas was introduced by maintaining the total background pressure of 45 Torr with the CH_4/H_2 ratio 1:4 (flow rate of CH_4 was 50 ± 1 and that of H_2 was 200 ± 1 sccm) for performing the graphene growth for 15 min on a catalytic copper substrate. Finally, the cooling process was performed quickly at a rate of 1° min^{-1} by opening the split furnace. Methane gas flow was stopped during the cooling process to stop the growth process. However, the cooling process was performed in the presence of argon and hydrogen gases. The pressure inside the CVD reactor during the growth was varied by varying individual hydrogen pressure or by varying individual methane pressure. First, hydrogen partial pressure was varied as 0.5 ± 0.2, 3 ± 0.2, 8 ± 0.2, 13 ± 0.2, and 18 ± 0.2 Torr, and second, methane partial pressure was varied as 7 ± 0.2, 12 ± 0.2, 22 ± 0.2, 32 ± 0.2, and 42 ± 0.2 Torr while maintaining the CH_4/H_2 ratio to 1:4. Growth time was reduced to 2 min to get graphene domains for calculating nucleation density during the growth. Several statistical runs were performed to validate the partial pressure-based process to confirm the quality and reproducibility of SLG. Table 1 indicates partial pressure of individual gases inside the quartz tube during graphene growth.

4.2. Transfer of Graphene on Si/SiO_2. After successful growth of graphene by LPCVD on the copper foil, the polymer layer of poly(methyl methacrylate) (PMMA) was spin-coated with 4000 rpm for 60 s on the graphene obscured copper foil. The copper foil covered with the PMMA layer floated on the ammonium persulphate solution to carry out etching of the beneath copper foil. Finally, the graphene-coated PMMA layer left on the surface of the solution was washed three times with DI water and scooped out on Si/SiO_2. Eventually, the polymer layer was dissolved by immersing the sample in acetone to leave behind only graphene on the Si/SiO_2 substrate.

4.3. Device Fabrication. The device was fabricated on graphene after cleaning and wrinkle-free transfer of graphene on Si/SiO_2. Lithography and e-beam technique were used to fabricate Au/Cr electrodes on graphene where thicknesses of Au and Cr were 60 and 10 nm, respectively.

4.4. Characterization Techniques. LPCVD-grown graphene was characterized using an Olympus MX51 industrial inspection optical microscope to take optical images of grown graphene in bright field mode. The Raman spectroscopy technique was employed for confirming and analyzing the graphene quality as well as number of layers present in graphene grown by the LPCVD method. Raman experiments were performed using a Renishaw inVia Raman spectrophotometer using a laser of 514.5 nm wavelength and 2.5 mW power with a 50× resolution of the objective lens. Scanning Electron Microscopy (SEM) with model Zeiss EVO MA-10 and resolution of 3 nm SEI MODE has been performed at 300 kV accelerating voltage on graphene grains to calculate nucleation density of graphene nuclei.

ASSOCIATED CONTENT

Supporting Information

The Supporting Information is available free of charge at https://pubs.acs.org/doi/10.1021/acsomega.0c02132.

Optical images of graphene on Si/SiO_2 at different (a−e) hydrogen partial pressures (SH1−SH5) and (f−j) and methane partial pressures (SC1−SC5) (resolution 20×), SEM images of graphene on Si/SiO_2 at different (a−e) hydrogen partial pressures (SH1−SH5) and (f−j) and methane partial pressures (SC1−SC5), scale bars are 50 μm, and nucleation density of graphene at different hydrogen partial pressures (SH1−SH5) and methane partial pressures (SC1−SC5), Raman spectra of CVD graphene grains after transfer on the Si/SiO_2 substrate at different (a) hydrogen partial pressures (SH1−SH5) and (b) methane partial pressures (SC1−SC5), comparative Raman data analysis of graphene grains at different hydrogen partial pressures (SH1−SH5) and methane partial pressures (SC1−SC5) (PDF)

AUTHOR INFORMATION

Corresponding Authors

Indu Sharma − *Photonic Materials Metrology Sub Division, Advanced Materials and Device Metrology Division, CSIR—National Physical Laboratory, 110012, India*; Email: indusharma.86@gmail.com

Bipin Kumar Gupta − *Photonic Materials Metrology Sub Division, Advanced Materials and Device Metrology Division, CSIR—National Physical Laboratory, 110012, India; Academy of Scientific and Innovative Research (AcSIR), Ghaziabad 201002, India*; orcid.org/0000-0002-0176-0007; Email: bipinbhu@yahoo.com

Authors

Girija Shankar Papanai − *Photonic Materials Metrology Sub Division, Advanced Materials and Device Metrology Division, CSIR—National Physical Laboratory, 110012, India; Academy of Scientific and Innovative Research (AcSIR), Ghaziabad 201002, India*

Sharon Jyotika Paul − *Photonic Materials Metrology Sub Division, Advanced Materials and Device Metrology Division, CSIR—National Physical Laboratory, 110012, India; Department of Chemistry, Institute of Basic Science, Bundelkhand University, Jhansi, Uttar Pradesh 284128, India*

Complete contact information is available at:

https://dx.doi.org/10.1021/acsomega.0c02132
ACS Omega 2020, 5, 22109−22118

https://pubs.acs.org/10.1021/acsomega.0c02132

Author Contributions

The manuscript was written through contributions of I.S., G.S.P., and S.J.P. All authors have given approval to the final version of the manuscript. I.S. designed and performed all of the experiments. B.K.G advised during all stages of the research and checked the manuscript.

Notes

The authors declare no competing financial interest.

■ ACKNOWLEDGMENTS

The authors would like to thank Director Dr. D. K. Aswal for encouraging them to carry research work on single-layer graphene metrology at CSIR-NPL. I.S. and G.S.P. would like to thank Council of Scientific and Industrial Research (CSIR) for providing fellowship through research associate (RA) and senior research fellowship (SRF), respectively. S.J.P. is also grateful to the Department of Science and Technology (DST) for providing fellowship through INSPIRE junior research fellowship (JRF).

■ REFERENCES

(1) Noorden, R. V. Chemistry: the trials of new carbon. *Nat. News* **2011**, *469*, 14−16.
(2) Lin, Y.-M.; Dimitrakopoulos, C.; Jenkins, K. A.; Farmer, D. B.; Chiu, H.-Y.; Grill, A.; Avouris, Ph. 100-GHz transistors from wafer-scale epitaxial graphene. *Science* **2010**, *327*, 662.
(3) Cohen-Karni, T.; Qing, Q.; Li, Q.; Fang, Y.; Lieber, C. M. Graphene and nanowire transistors for cellular interfaces and electrical recording. *Nano Lett.* **2010**, *10*, 1098−1102.
(4) Du, X.; Skachko, I.; Barker, A.; Andrei, E. Y. Approaching ballistic transport in suspended graphene. *Nat. Nanotechnol.* **2008**, *3*, 491−495.
(5) Zhan, B.; Li, C.; Yang, J.; Jenkins, G.; Huang, W.; Dong, X. Graphene Field-Effect Transistor and Its Application for Electronic Sensing. *Small* **2014**, *10*, 4042−4065.
(6) Novoselov, K. S.; Jiang, D.; Schedin, F.; Booth, T. J.; Khotkevich, V. V.; Morozov, S. V.; Geim, A. K. Two-dimensional atomic crystals. *Proc. Natl. Acad. Sci. U.S.A.* **2005**, *102*, 10451−10453.
(7) Blake, P.; Brimicombe, P. D.; Nair, R. R.; Booth, T. J.; Jiang, D.; Schedin, F.; Ponomarenko, L. A.; Morozov, S. V.; Gleeson, H. F.; Hill, E. W.; Geim, A. K.; Novoselov, K. S. Graphene-based liquid crystal device. *Nano Lett.* **2008**, *8*, 1704−1708.
(8) Stankovich, S.; Dikin, D. A.; Piner, R. D.; Kohlhaas, K. A.; Kleinhammes, A.; Jia, Y.; Wu, Y.; Nguyen, S. T.; Ruoff, R. S. Synthesis of graphene-based nanosheets via chemical reduction of exfoliated graphite oxide. *Carbon* **2007**, *45*, 1558−1565.
(9) Eda, G.; Fanchini, G.; Chhowalla, M. Large-area ultrathin films of reduced graphene oxide as a transparent and flexible electronic material. *Nat. Nanotechnol.* **2008**, *3*, 270−274.
(10) Li, D.; Müller, M. B.; Gilje, S.; Kaner, R. B.; Wallace, G. G. Processable aqueous dispersions of graphene nanosheets. *Nat. Nanotechnol.* **2008**, *3*, 101−105.
(11) Berger, C.; Song, Z.; Li, T.; Li, X.; Ogbazghi, A. Y.; Feng, R.; Dai, Z.; Marchenkov, A. N.; Conrad, E. H.; First, P. N.; De Heer, W. A. Ultrathin epitaxial graphite: 2D electron gas properties and a route toward graphene-based nanoelectronics. *J. Phys. Chem. B* **2004**, *108*, 19912−19916.
(12) Berger, C.; Song, Z.; Li, X.; Wu, X.; Brown, N.; Naud, C.; Mayou, D.; Li, T.; Hass, J.; Marchenkov, A. N.; Conrad, E. H. Electronic confinement and coherence in patterned epitaxial graphene. *Science* **2006**, *312*, 1191−1196.
(13) Yi, P.; Dong-Xia, S.; Hong-Jun, G. Formation of graphene on Ru (0001) surface. *Chin. Phys.* **2007**, *16*, 3151−3153.
(14) Sutter, P. W.; Flege, J. I.; Sutter, E. A. Epitaxial graphene on ruthenium. *Nat. Mat.* **2008**, *7*, 406−411.
(15) Li, X.; Cai, W.; An, J.; Kim, S.; Nah, J.; Yang, D.; Piner, R.; Velamakanni, A.; Jung, I.; Tutuc, E.; Banerjee, S. K. Large-area synthesis of high-quality and uniform graphene films on copper foils. *Science* **2009**, *324*, 1312−1314.
(16) Kim, K. S.; Zhao, Y.; Jang, H.; Lee, S. Y.; Kim, J. M.; Kim, K. S.; Ahn, J. H.; Kim, P.; Choi, J. Y.; Hong, B. H. Large-scale pattern growth of graphene films for stretchable transparent electrodes. *Nature* **2009**, *457*, 706−710.
(17) Reina, A.; Jia, X.; Ho, J.; Nezich, D.; Son, H.; Bulovic, V.; Dresselhaus, M. S.; Kong, J. Large area, few-layer graphene films on arbitrary substrates by chemical vapor deposition. *Nano Lett.* **2009**, *9*, 30−35.
(18) Reina, A.; Thiele, S.; Jia, X.; Bhaviripudi, S.; Dresselhaus, M. S.; Schaefer, J. A.; Kong, J. Growth of large-area single-and bi-layer graphene by controlled carbon precipitation on polycrystalline Ni surfaces. *Nano Res.* **2009**, *2*, 509−516.
(19) Yu, Q.; Lian, J.; Siriponglert, S.; Li, H.; Chen, Y. P.; Pei, S. S. Graphene segregated on Ni surfaces and transferred to insulators. *Appl. Phys. Lett.* **2008**, *93*, No. 113103.
(20) Kashyap, P. K.; Sharma, I.; Gupta, B. K. Continuous Growth of Highly Reproducible Single-Layer Graphene Deposition on Cu Foil by Indigenously Developed LPCVD Setup. *ACS Omega* **2019**, *4*, 2893−2901.
(21) Vlassiouk, I.; Smirnov, S.; Regmi, M.; Surwade, S. P.; Srivastava, N.; Feenstra, R.; Eres, G.; Parish, C.; Lavrik, N.; Datskos, P.; Dai, S. Graphene nucleation density on copper: fundamental role of background pressure. *J. Phys. Chem. C* **2013**, *117*, 18919−18926.
(22) Cheng, Y.; Bi, H.; Che, X.; Li, D.; Ji, W.; Huang, F. Suppression of graphene nucleation by plasma treatment of Cu foil for the rapid growth of large-size single-crystal graphene. *Carbon* **2019**, *147*, 51−57.
(23) Li, X.; Magnuson, C. W.; Venugopal, A.; Tromp, R. M.; Hannon, J. B.; Vogel, E. M.; Colombo, L.; Ruoff, R. S. Large-area graphene single crystals grown by low-pressure chemical vapor deposition of methane on copper. *J. Am. Chem. Soc.* **2011**, *133*, 2816−2819.
(24) Ago, H.; Ogawa, Y.; Tsuji, M.; Mizuno, S.; Hibino, H. Catalytic growth of graphene: toward large-area single-crystalline graphene. *J. Phys. Chem. Lett.* **2012**, *3*, 2228−2236.
(25) Withanage, S.; Nanayakkara, T.; Gunawardana, B.; Munasinghe, C. R.; Wijewardena, U. K.; Samaraweera, R.; Kriisa, A.; Mani, R. The effect of multi-step Cu surface oxidization on growth of single crystal graphene by low pressure chemical vapor deposition. *APS Meeting Abstracts* **2019**, E13−002.
(26) Kang, J.; Lee, C. J.; Kim, J.; Park, H.; Lim, C.; Lee, J.; Choi, M.; Park, H. Effect of copper surface morphology on grain size uniformity of graphene grown by chemical vapor deposition. *Curr. Appl. Phys.* **2019**, *19*, 1414−1420.
(27) Bhaviripudi, S.; Jia, X.; Dresselhaus, M. S.; Kong, J. Role of kinetic factors in chemical vapor deposition synthesis of uniform large area graphene using copper catalyst. *Nano Lett.* **2010**, *10*, 4128−4133.
(28) Blake, P.; Hill, E. W.; Castro Neto, A. H.; Novoselov, K. S.; Jiang, D.; Yang, R.; Booth, T. J.; Geim, A. K. Making graphene visible. *Appl. Phys. Lett.* **2007**, *91*, No. 063124.
(29) Giannazzo, F.; Sonde, S.; Raineri, V.; Patanè, G.; Compagnini, G.; Aliotta, F.; Ponterio, R.; Rimini, E. Optical, morphological and spectro-scopic characterization of graphene on SiO_2. *Phys. Status Solidi C* **2010**, *7*, 1251−1255.
(30) Ferrari, A. C.; Meyer, J. C.; Scardaci, V.; Casiraghi, C.; Lazzeri, M.; Mauri, F.; Piscanec, S.; Jiang, D.; Novoselov, K. S.; Roth, S.; Geim, A. K. Raman spectrum of graphene and graphene layers. *Phys. Rev. Lett.* **2006**, *97*, No. 187401.
(31) Malard, L. M.; Pimenta, M. A.; Dresselhaus, G.; Dresselhaus, M. S. Raman spectroscopy in graphene. *Phys. Rep.* **2009**, *473*, 51−87.
(32) Kozlov, G. I.; Knorre, V. G. Single-pulse shock tube studies on the kinetics of the thermal decomposition of methane. *Combust. Flame* **1962**, *6*, 253−263.

(33) Li, G.; Huang, S. H.; Li, Z. Gas-phase dynamics in graphene growth by chemical vapour deposition. *Phys. Chem. Chem. Phys.* **2015**, *17*, 22832−22836.
(34) Venables, J. A.; Spiller, G. D. Nucleation and Growth of Thin Films, Surface Mobilities on Solid Materials—Fundamental Conceptsand Applications. *NATO ASI Series, Series B: Physics*, Binh, V. T.; Binh, V. T., Eds.; 1983; *86*, 341.
(35) Geng, D.; Wu, B.; Guo, Y.; Huang, L.; Xue, Y.; Chen, J.; Yu, G.; Jiang, L.; Hu, W.; Liu, Y. Uniform hexagonal graphene flakes and films grown on liquid copper surface. *Proc. Natl. Acad. Sci. U.S.A.* **2012**, *109*, 7992−7996.
(36) Geng, D.; Meng, L.; Chen, B.; Gao, E.; Yan, W.; Yan, H.; Luo, B.; Xu, J.; Wang, H.; Mao, Z.; Xu, Z. Controlled Growth of Single-Crystal Twelve-Pointed Graphene Grains on a Liquid Cu Surface. *Adv. Mater.* **2014**, *26*, 6423−6429.
(37) (a) Liu, Y.; Wu, T.; Yin, Y.; Zhang, X.; Yu, Q.; Searles, D. J.; Ding, F.; Yuan, Q.; Xie, X. How low nucleation density of graphene on CuNi alloy is achieved. *Advanced Science* **2018**, *5*, No. 1700961. (b) Markov, I. V. *Crystal Growth for Beginners: Fundamentals of Nucleation, Crystal Growth and Epitaxy*, 2nd ed.; World Scientific, 2003.
(38) Sharma, I.; Dhakate, S. R.; Subhedar, K. M. CVD growth of continuous and spatially uniform single layer graphene across the grain boundary of preferred (111) oriented copper processed by sequential melting−resolidification−recrystallization. *Mater. Chem. Front.* **2018**, *2*, 1137−1145.
(39) Zhang, W.; Ping, W.; Zhenyu, L.; Jinlong, Y. First-principles thermodynamics of graphene growth on Cu surfaces. *J. Phys. Chem. C* **2011**, *115*, 17782−17787.
(40) Gupta, B. K.; Tiwari, R. S.; Srivastava, O. N. Studies on synthesis and hydrogenation behaviour of graphitic nanofibres prepared through palladium catalyst assisted thermal cracking of acetylene. *J. Alloys Compd.* **2004**, *381*, 301−308.
(41) Vlassiouk, I.; Murari, R.; Pasquale, F.; Sheng, D.; Panos, D.; Gyula, E.; Sergei, S. Role of hydrogen in chemical vapor deposition growth of large single-crystal graphene. *ACS Nano* **2011**, *5*, 6069−6076.
(42) Zhang, Y.; Zhen, L.; Pyojae, K.; Luyao, Z.; Chongwu, Z. Anisotropic hydrogen etching of chemical vapor deposited graphene. *ACS Nano* **2012**, *6*, 126−132.
(43) Yu, Q.; Jauregui, L. A.; Wu, W.; Colby, R.; Tian, J.; Su, Z.; Cao, H.; Liu, Z.; Pandey, D.; Wei, D.; Chung, T. F. Control and characterization of individual grains and grain boundaries in graphene grown by chemical vapour deposition. *Nat. Mater.* **2011**, *10*, 443−449.
(44) Li, X.; Magnuson, C. W.; Venugopal, A.; An, J.; Suk, J. W.; Han, B.; Borysiak, M.; Cai, W.; Velamakanni, A.; Zhu, Y.; Fu, L. Graphene films with large domain size by a two-step chemical vapor deposition process. *Nano Lett.* **2010**, *10*, 4328−4334.
(45) Zhang, Y.; Tan, Y. W.; Stormer, H. L.; Kim, P. Experimental observation of the quantum Hall effect and Berry's phase in graphene. *Nature* **2005**, *438*, 201−204.

NOTE ADDED AFTER ASAP PUBLICATION

This paper was published on August 26, 2020. Due to production error, Table 5 contained incorrect information and an affiliation was incorrect. The corrected version was reposted on August 27, 2020.

https://dx.doi.org/10.1021/acsomega.0c02132
ACS Omega 2020, 5, 22109−22118